Deposition Kinetics of Two Viruses in Packed Beds of Quartz Granular Media

ARTICLE *in* LANGMUIR · NOVEMBER 1996

Impact Factor: 4.46 · DOI: 10.1021/la950884d

3 AUTHORS, INCLUDING:

Terese Olson
University of Michigan
28 PUBLICATIONS **1,089** CITATIONS
SEE PROFILE

Stanley Grant
University of California, Irvine
77 PUBLICATIONS **2,061** CITATIONS
SEE PROFILE

Research Article

Deposition Kinetics of Two Viruses in Packed Beds of Quartz Granular Media

Samuel L. Penrod, Terese M. Olson, and Stanley B. Grant

Langmuir, **1996**, 12 (23), 5576-5587 • DOI: 10.1021/la950884d

Deposition Kinetics of Two Viruses in Packed Beds of Quartz Granular Media

Samuel L. Penrod, Terese M. Olson, and Stanley B. Grant*

Department of Civil and Environmental Engineering, University of California, Irvine, Irvine, California 92697

Received October 17, 1995. In Final Form: August 15, 1996[⊗]

The removal of waterborne viruses by packed bed filtration was examined using a model system consisting of two different bacteriophages (MS2 and λ) and saturated beds of ultrapure quartz grains. The majority of these experiments were conducted at a solution pH of 5, where the viruses and quartz possess a net negative surface charge. On the basis of a simple model that correctly predicts the isoelectric point (p*I*) of MS2, the surface charge on this virus appears to originate from the ionization of amino acid residues located on the exterior of the virus particle. The deposition rates of both MS2 and λ at pH 5 are sensitive to the ionic composition of the suspending fluid, with more rapid filtration occurring at the higher salt concentrations. The filtration rate of λ approaches the theoretical value estimated using the Smoluchowski−Levich (S−L) approximation at pH 5 and high salt concentrations (300 mM NaCl) or at the p*I* of the virus, suggesting that electrostatic repulsive forces effectively dominate the filtration dynamics of λ. The filtration rate of MS2, on the other hand, is at least 800% less than the theoretical S−L value at high salt or at the p*I* of this virus, suggesting that both electrostatic and nonelectrostatic repulsive forces influence the filtration of MS2. We investigate the possibility that this nonelectrostatic force is steric in nature, arising from hydrophilic polypeptide loops which extend a maximum of 1 nm off the MS2 surface.

Introduction

Virus particles are constructed from a core nucleic acid (either DNA or RNA) surrounded by a protein coat (the capsid) and, in some cases, a lipid outer coating. In many respects, viruses resemble amphoteric colloidal particles routinely studied in colloid science. When suspended in an aqueous environment, acidic and/or basic functional groups associated with a virus can ionize, giving rise to a net charge on the viral surface that is pH dependent.[1,2] This surface charge influences virus partitioning to solid−liquid interfaces in a diverse array of biological phenomena, including the removal of viral pathogens from water by coagulation[3−6] and filtration,[7,8] detection of human viruses in clinical samples,[9] the adsorption of viruses to soils and minerals,[10−15] and even the binding of viruses to receptor sites on host cells.[16,17] Classical Derjaguin−Landau−Verwey−Overbeek (DLVO) potential energy calculations, which describe the balance of electrostatic repulsion and van der Waals attraction forces as a function of virus−mineral separation distance, have been used successfully in the case of the polio virus[18] and bacteriophage PRD1[19] to describe their sorption behavior on mineral surfaces. But while it is relatively well established that electrostatic and van der Waals forces are important, it is less clear whether other interaction forces—including hydrophobic, hydration, and steric interactions—affect the partitioning of viruses onto solid surfaces.

In this study we investigated the filtration kinetics of two viruses (MS2 and λ) in a model porous medium consisting of saturated beds of ultrapure quartz sand. Both of these viruses are "bacteriophages", a class of viruses that infect bacteria. They were chosen for this study because their molecular structure is well characterized, and they differ significantly with respect to their size, shape, and electrostatic properties (see Figure 1). Using a modified electrophoresis technique developed recently in our laboratory for small viruses such as MS2,[1] a more fundamental understanding of the contribution of repulsive electrostatic forces to virus filtration is now possible. The filtration efficiency and electrophoretic mobility of these two viruses were measured over a range of solution pH and ionic strength conditions, and these data were interpreted in terms of the atomic-level three-dimensional structure of the respective viruses. A relatively hydrophilic, negatively-charged collector surface, quartz sand, was chosen because the focus of this study was to identify the repulsive forces that promote virus transport in porous media. Consequently, the importance of attractive hydrophobic forces was not examined, although they have been implicated in the capture of viruses onto more hydrophobic surfaces.[20−22]

* Author to whom all correspondence should be addressed.

[⊗] Abstract published in *Advance ACS Abstracts,* October 15, 1996.

(1) Penrod, S. L.; Olson, T. M.; Grant, S. B. *J. Colloid Interface Sci.* **1995**, *173*, 521.
(2) Taylor, D. H.; Bosmann, H. B. *J. Colloid Interface Sci.* **1981**, *83*, 153.
(3) York, D. L.; Drewry, W. A. *J.—Am. Water Works Assoc.* **1974**, 711.
(4) Grant, S. B. *Environ. Sci. Technol.* **1994**, *28*, 928.
(5) Floyd, R.; Sharp, D. G. *Appl. Environ. Microbiol.* **1976**, *33*, 159.
(6) Floyd, R.; Sharp, D. G. *Appl. Environ. Microbiol.* **1978**, *35*, 1084.
(7) Gilgen, M.; Wegmuller, B.; Burkhalter, P.; Buhler, H.-P.; Muller, U.; Luthy, J.; Candrian, U. *Appl. Environ. Microbiol.* **1995**, *61*, 1226.
(8) Gerba, C. P. In *Methods for Recovering Viruses from the Environment*; Berg, G., Ed.; CRC Press: Boca Raton, FL, 1987; Chapter 1.
(9) Duverlie, G.; Houbart, L.; Visse, B.; Chomel, J. J.; Manuguerra, J. C.; Hannoun, C.; Orfila, J. *J. Virol. Methods* **1992**, *40*, 77.
(10) Duboise, S. M.; Moore, B. E.; Sagik, B. P. *Appl. Environ. Microbiol.* **1976**, *31*, 536.
(11) Lance, J. C.; Gerba, C. P.; Melnick, J. L. *Appl. Environ. Microbiol.* **1976**, *32*, 520.
(12) Taylor, D. H.; Moore, R. S.; Sturman, L. S. *Appl. Environ. Microbiol.* **1981**, *42*, 976.
(13) Moore, R. S.; Taylor, D. H.; Sturman, L. S.; Reddy, M. M.; Fuhs, G. W. *Appl. Environ. Microbiol.* **1981**, *42*, 963.
(14) Gerba, C. P.; Sobsey, M. D.; Wallis, C.; Melnick, J. L. *Environ. Sci. Technol.* **1975**, *9*, 727.
(15) Grant, S. B.; List, E. J.; Lidstrom, M. E. *Water Resour. Res.* **1993**, *29*, 2067.
(16) Flynn, S. J.; Ryan, P. *J. Virol.* **1995**, *69*, 834.
(17) Ye, Z.; Sun, W.; Suryanarayana, K.; Justice, P.; Robinson, D.; Wagner, R. R. *J. Virol.* **1994**, *68*, 7386.
(18) Murray, J. P.; Parks, G. A. ACS Symposium Series 189; Kavanaugh, M. C., Leckie, J. O., Eds.; American Chemical Society: Washington, DC, 1980.
(19) Loveland, J. P.; Ryan, J. N.; Amy, G. L.; Harvey, R. W. *Colloids Surf., A* **1996**, *107*, 205.

S0743-7463(95)00884-5 CCC: $12.00

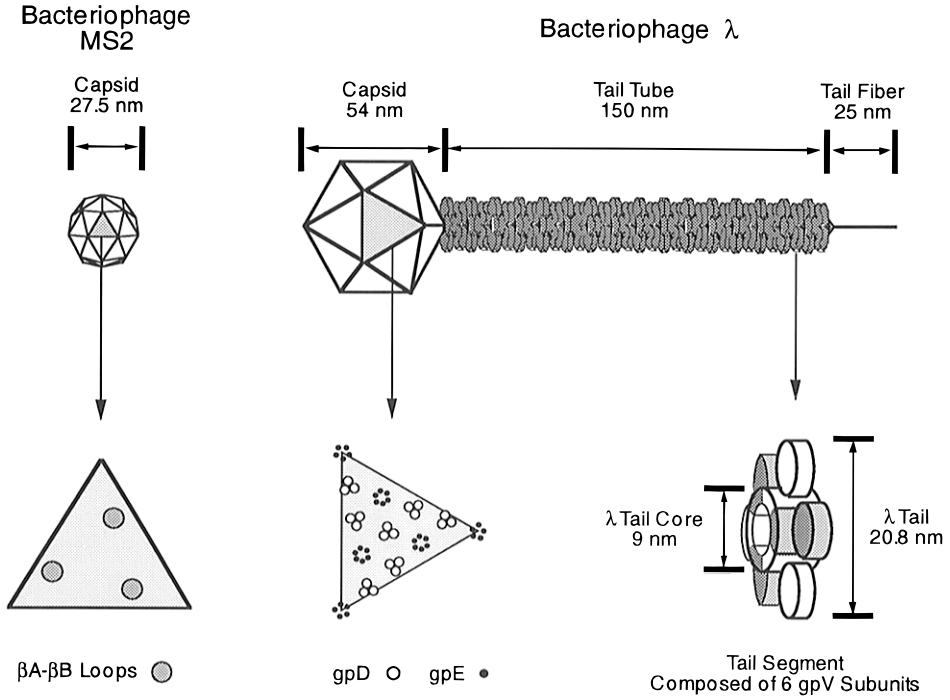

Figure 1. Structural characteristics of the two viruses used in this study. The MS2 capsid is constructed from 60 identical triangular units, each of which consists of three copies of a single polypeptide. The approximate location of the βA−βB loops on each triangular unit are indicated in the expanded view (see text). The capsid surface of bacteriophage λ is constructed from 405 copies each of two proteins, gpE and gpD. The expanded view illustrates the distribution of outward-protruding portions of gpE and gpD on the capsid surface (adapted from Casjens and Hendrix[47]). The tail tube of λ is constructed from 32 segments, each of which consists of 6 gpV protein subunits. The carboxyl and amino portions of the gPV polypeptide form the interior and exterior portions of the tail tube, respectively, as illustrated in the expanded view.

We find that the filtration of λ is influenced primarily by electrostatic repulsive interactions that develop between amino acid residues present on the capsid surface and the negatively-charged quartz media. The filtration of MS2, on the other hand, appears to be influenced by both electrostatic and steric repulsive forces, with the latter arising from interactions between the quartz surface and hydrophilic polypeptide loops that extend off of the capsid surface. Our experiments suggest that different repulsive forces may be involved in the partitioning of viruses to solid−liquid interfaces, depending on the macroscopic and atomic-level structure of a particular virus and its surface electrical properties.

Experimental Section

Growth and Measurement of Virus Particles. The bacteriophages lambda (λ) and MS2 were grown on the *E. coli* hosts C600 and ATCC 15597, respectively. Strain cI47 of λ was prepared by the method of low multiplicity and purified by centrifugation in a CsCl gradient.[23] MS2 was prepared using the method of Bales *et al.*[22] and then further purified by CsCl gradient centrifugation. Stocks of λ and MS2 were stored at 4 °C in standard salt buffer (SM) [0.05 M tris[hydroxymethyl]-aminomethane (base), 0.1 M NaCl, 0.008 M $MgSO_4 \cdot 7H_2O$, and 0.01% gelatin adjusted to pH 7.5 with 12 N HCl] and Tris buffer [0.04 M tris(hydroxymethyl)aminomethane (base), 0.22 M NaCl, 0.008 M KCl, and 0.0006 M Na_2HPO_4 adjusted to pH 7.4 with 12 N HCl], respectively.

Concentrations of infective viruses were determined by the plaque-forming unit (PFU) assay. Dilutions of each sample were mixed with host cells, plated on nutrient agar, and incubated following standard procedures.[24] The resulting plaque counts were converted to PFU/mL.

Microelectrophoresis Measurements. The surface electrostatic properties of the two viruses were measured using whole-particle microelectrophoresis. Prior to electrophoresis measurements, the virus stock was purified by membrane dialysis. One microliter of virus stock in SM or Tris buffer was diluted into 5 mL of filtered (0.22 μm Nalgene surfactant-free) electrolyte solution. The virus solution was dialyzed four times against 3 L of electrolyte solution in Spectra/Por 15,000 tubing (Spectrum Medical Industries, Inc.). Electrolyte solutions were prepared from deionized water (Milli-Q water, 18 MΩcm, Millipore, Inc.), analytical grade NaCl, $NaHCO_3$ (pH > 7), and HCl (pH < 7). Sodium bicarbonate solutions were equilibrated with the atmosphere for 24 h. All solutions and glassware were sterilized prior to use.

Microelectrophoresis measurements were conducted at 8 °C using a Rank Brothers (Bottisham, Cambridge, U.K.) Mark II apparatus equipped with a 0.5 mW green 544 nm wavelength He−Ne laser (Melles Griot Model O5 SGR 851). In an earlier study in our laboratory, it was determined that virus particles as small as MS2 could be visualized in a conventional capillary microelectrophoresis cell if the particles were illuminated with a green laser. Details of the method are reported elsewhere.[1] The ζ potentials of the virus particles were calculated from the measured electrophoretic mobilities using analytical expressions that are described by Hunter.[25]

Filtration Experiments. Filtration experiments were carried out at 4 °C using ultrapure quartz grains (Unimin, New Canaan, CT) with an average grain size of 200 μm as the packing material. Details of the quartz size fractionation, cleaning, and preparation procedures are described elsewhere.[26] Fresh clean quartz was used for each experiment, and bed porosities were determined gravimetrically at the end of each experiment. Filtration rates were characterized in terms of the breakthrough

(20) Shields, P. A.; Farrah, S. R. *Appl. Environ. Microbiol.* **1983**, *45*, 526.
(21) Mix, T. W. In *Methods for Recovering Viruses from the Environment*; Berg, G., Ed.; CRC Press: Boca Raton, FL, 1987; Chapter 7.
(22) Bales, R. C.; Hinkle, S. R.; Kroeger, T. W.; Stocking, K. *Environ. Sci. Technol.* **1991**, *25*, 2088.
(23) Sambrook, J.; Gritsch, E. F.; Maniatis, R. *Molecular Cloning*; Cold Spring Harbor Laboratory Press: Plainview, NY, 1989.
(24) Adams, M. H. *Bacteriophage*; Interscience Publication: New York, 1959.
(25) Hunter, R. J. *Zeta Potential in Colloid Science*; Academic Press: New York, 1981.
(26) Litton, G.; Olson, T. M. *Environ. Sci. Technol.* **1993**, *27*, 185.

concentration of infective virus particles (PFU/mL) in the column effluent. Glass columns (1.6 cm, Pharmacia LKB C16 with adjustable height adapters) were packed by allowing the quartz to settle in filtered deionized water at room temperature. Column lengths were adjusted for each experiment to obtain the necessary resolution of effluent breakthrough concentrations; in particular, only normalized breakthrough concentrations, PFU/PFU_0, less than 0.9 were used to calculate virus deposition rates, where PFU_0 represents the infective particle concentration in the column influent. Prior to each experiment, columns packed with quartz grains were equilibrated with the electrolyte buffer by pumping (Pharmacia LKB P1 peristaltic pump) at least 10 pore volumes of electrolyte solution through the column. Suspension flow rates were approximately 3 mL/min, which is equivalent to a superficial velocity of 0.025 cm s^{-1}. A fraction collector (Pharmacia LKB FRAC-200) was programmed to collect 9 mL of column effluent per tube. Control experiments were performed to ensure that virus adsorption to the column walls did not occur in our system.

Modeling of Filtration Data. The column breakthrough data were analyzed using the linear chromatography model:[27]

$$\frac{\partial n}{\partial t} = -U_i \frac{\partial n}{\partial z} - \frac{3(1-\epsilon)}{\epsilon a_g}\frac{\partial n_s}{\partial t} \tag{1a}$$

$$\frac{\partial n_s}{\partial t} = k_f n - k_r n_s \tag{1b}$$

where n is the concentration of infective virus particles in the pore fluid in units of PFU/mL, n_s is the concentration of deposited virus in units of PFU/area of grain, t is time, z is the distance from the column influent, ϵ is the bed porosity, U_i is the interstitial particle velocity (equal to U/ϵ, where U is the superficial velocity obtained as the volumetric flow rate divided by the cross-sectional area of the bed), and a_g is the radius of the bed grains. Equation 1a relates the temporal change in local virus concentration in the pore fluid (left hand term) to interstitial advective transport of the virus (first term on the right hand side) and deposition of the virus onto the collector surface (second term on the right hand side). Hydrodynamic dispersion and molecular diffusion are not considered in the derivation of eq 1a, because the interstitial transport of virus particles is advection-dominated under the set of conditions employed in this study.[28] Equation 1b describes the rate at which viruses are removed from the pore fluid by deposition on the collector surface. The forward rate constant k_f accounts for the adsorption of viruses onto the collector surface, and the reverse rate constant k_r accounts for particle detachment. This model applies under "clean-bed conditions" where the deposition rate is not influenced by previously deposited particles.[29]

For each filtration experiment, values of k_f and k_r were determined by fitting an integrated form of eqs 1a and 1b to the breakthrough data using a Levenberg−Marquardt nonlinear least-squares approach.[30] To determine if the reverse rate constant k_r was needed for a particular filtration experiment, the breakthrough data was also fit to a simpler model in which particle deposition is assumed to occur irreversibly.[27] If the difference in the χ^2 values obtained for the two models was statistically insignificant (as judged by the F-test[31]), then the simpler irreversible deposition model was adopted.

The fraction of the quartz surface covered by deposited particles was estimated as $\theta = n_s s_v$, where s_v represents the projected area of each virus, taken to be 5.3×10^{-12} and 8.1×10^{-11} cm^2 for MS2 and λ, respectively.

Calculation of Attachment Efficiencies. Values for the attachment efficiency α were calculated from the forward rate constant k_f using the following expression

$$\alpha = \frac{4.0 k_f}{U \eta_0} \tag{2}$$

where η_0 is the "dimensionless deposition rate" [32] in the absence of repulsive forces. Two different approaches were used to estimate η_0. A theoretical expression for η_0 can be derived under conditions where Brownian diffusion dominates the transport of particles in the immediate vicinity of the collector surface and where colloidal and hydrodynamic interactions between the virus and collector surface are negligible (the so-called Smoluchowski−Levich or "S−L" approximation)[33]

$$\eta_0 = 4.0 A_s^{1/3}\left(\frac{D_\infty}{2a_g U}\right)^{2/3} \tag{3}$$

In eq 3, A_s is Happel's dimensionless porosity-dependent parameter,[34−36] and D_∞ is the diffusion coefficient of the colloid (i.e., virus) in bulk solution, which we estimated for each virus from the Stokes−Einstein equation.[37] For the two viruses used in this study, deposition rates calculated from eq 3 were within 25% of η_0 values estimated from a numerical model published by Elimelech and co-workers,[38,39] which accounts for the influence of van der Waals and hydrodynamic forces on particle deposition rates.

Strictly speaking, eq 3 applies to systems where both the colloid and the collector are perfect spheres. With regard to the nonspherical nature of the quartz grain media, previous studies[40] with this packing material have shown close agreement between experimentally determined deposition rates of 245 nm diameter polystyrene latex microspheres and values of η_0 calculated from eq 3. The spherical assumption is probably valid in the case of MS2 but is not satisfied in the case of λ (see Figure 1). Despite the nonspherical morphology of λ, however, we found that experimentally observed deposition rates were close to those predicted by eq 3 (see Results and Discussion). Theoretical dimensionless deposition rates were calculated for both MS2 and λ from eq 3 assuming these viruses behave like spherical particles with radii of their capsids 14 and 27 nm, respectively.

The dimensionless deposition rates for the two viruses were also estimated experimentally by measuring the forward rate constant k_f under pH conditions where the viruses possess zero net charge (i.e., pH = p*I*). Under these conditions, electrostatic double-layer forces between the viruses and quartz grain media should be negligible. Provided that there are no other (non-electrostatic) repulsive forces governing colloid deposition rates, the attachment efficiency α should approach unity, and therefore experimental deposition rates can be calculated directly from measured values of the forward rate constant (k_f^{pI}) using a rearranged version of eq 2; namely,

$$\eta_0^{pI} = \frac{4 k_f^{pI}}{U} \tag{4}$$

Surface Charge Calculations. The electrostatic charge associated with specific polypeptides present on the surface of MS2 or λ was calculated using eq 5

$$\sigma = \{\sum_i R_i H^+ - \sum_i R_i O^-\} FN/A \tag{5}$$

where $\sum R_i H^+$ and $\sum R_i O^-$ represent, respectively, the number of

(27) Rajagopalan, R.; Chu, R. Q. *J. Colloid Interface Sci.* **1982**, *86*, 299.
(28) Penrod, S. L. Unpublished M.S. Dissertation, University of California, Irvine, 1995.
(29) Johnson, P. R.; Elimelech, M. *Langmuir* **1995**, *11*, 801.
(30) Press, W. H.; Flannery, B. P.; Teukolsky, S. A.; Vetterling, W. T. *Numerical Recipes*; Cambridge University Press: New York, 1986.
(31) Bevington, P. R.; Robinson, D. K. *Data Reduction and Error Analysis for the Physical Sciences*, 2nd ed.; McGraw-Hill, Inc.: New York, 1992.
(32) Yao, K.; Habibian, M. T.; O'Melia, C. R. *Environ. Sci. Technol.* **1971**, *5*, 1105.
(33) Spielman, L. A.; Friedlander, S. K. *J. Colloid Interface Sci.* **1974**, *46*, 22.
(34) Happel, J. *AIChE J.* **1958**, *4*, 197.
(35) Pfeffer, R. *Ind. Eng. Chem. Fundam.* **1964**, *3*, 380.
(36) Pfeffer, R. Happel, J. *AIChE J.* **1964**, *10*, 605.
(37) Levich, V. G. *Physicochemical Hydrodynamics*; Prentice Hall: Englewood Cliffs, NJ, 1962.
(38) Elimelech, M. *Sep. Technol.* **1994**, *4*, 186.
(39) Elimelech, M.; Song, L. ACS Symposium Series 491; Sabatini, D. A., Knox, R. C., Eds.; American Chemical Society: Washington, DC, 1992; Chapter 3.
(40) Litton, G. M. Unpublished Ph.D. Dissertation, University of California, Irvine, 1993.

Table 1. Charged Amino Acid Residues and Ionization Constants

	number/polypeptide				
amino acid	MS2[a]	λ tail[b]	λ tail fiber[b]	$pK_a^{a.a}$	pK_a^{prot}
glutamic acid	5 (1)	3	16	4.3	4.5
aspartic acid	4 (4)	2	21	3.9	4.5
arginine	4 (0)	1	18	12.5	13.0
lysine	6 (2)	4	22	10.8	10.1

[a] Values are given as the total number of amino acid residues on the MS2 capsid; values in parentheses are estimates of exterior amino acid residues as determined from three-dimensional images of the capsid (see text). [b] Values reflect estimates of the number of exterior amino acid residues, which are assumed to be located on the one-third portion of the gpV and gpJ polypeptides closest to the N-terminus (Hendrix, R. W. Personal communication).

positively and negatively charged amino acid residues per polypeptide, N is the number of polypeptides per viral particle ($N = 180$ for MS2), A is the surface area of the virus ($A = 2.4 \times 10^{-15}$ m^2/particle for MS2), and F is Faraday's constant. The summations in eq 5 are taken over all positively and negatively charged amino acid residues in the polypeptide chain. Positively charged residues in the first summation on the right hand side of eq 5 include protonated amine and diaminoiminium groups present on the side chains of lysine and arginine, respectively, and the α-NH_3^+ group on the N-terminus of the protein. Negatively charged residues included in eq 5 are carboxylate groups present on the side chains of aspartate and glutamate, and the α-COO^- group on the C-terminus of the protein. The fraction of these charged residues that are ionized at any particular pH was estimated from equilibrium calculations using two sets of previously published ionization constants listed in Table 1: one set, designated $pK_a^{a.a}$, corresponds to equilibrium constants measured for single amino acids, and the other set, designated pK_a^{prot}, are equilibrium constants estimated for amino acids embedded in a polypeptide chain.[41] Also shown in this table are the number of charged amino acid residues associated with the surface proteins of MS2 and λ.

Results and Discussion

Surface Properties of MS2. MS2 is a spherically shaped virus approximately 27 nm in diameter (see Figure 1). The virus lacks a lipid outer coating, and its capsid is constructed from 180 copies of a single polypeptide arranged on the viral surface in icosahedral symmetry. The capsid polypeptide is 129 amino acid residues in length,[42] and its three-dimensional structure has recently been determined to atomic-level resolution.[43,44] These high-resolution studies reveal that the capsid protein consists of a five-stranded β sheet that primarily faces the inside of the particle and two α helices and a hairpin loop that are present on the viral surface. The secondary structure of the capsid protein is indicated along the right hand side of Figure 2, where the solid and striped bars represent β sheets and α helices, respectively. Also shown in this figure are the relative hydrophobicity or "hydropathy" of the protein residues in the capsid, as calculated using a weighted sum algorithm published by Kyte and Doolittle.[45] The locations of amino acid residues that specifically interact with the viral RNA on the capsid interior[46] are also shown in Figure 2 (filled diamonds).

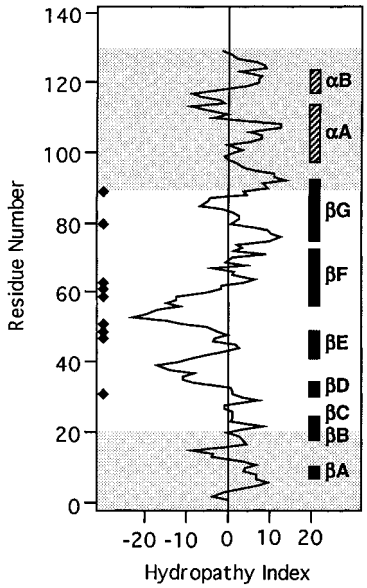

Figure 2. Secondary structure and calculated hydropathy index for the MS2 coat protein. Positive and negative hydropathy values indicate, respectively, hydrophobic and hydrophilic protein residues. The bars along the right hand side of the graph correspond to secondary structures determined from X-ray crystallography, including α helices (cross hatched bars) and β sheets (solid bars). Also shown are protein residues that are located on the exterior of the capsid (shaded regions of graph) and that specifically interact with encapsulated RNA (diamond symbols). Protein residues are numbered from the N-terminus of the polypeptide.

By examining three-dimensional images of the MS2 capsid protein constructed from X-ray diffraction data (see Figure 4 in ref 44), we were also able to classify each residue in the capsid protein as lying on either the exterior or the interior of MS2: residues in the approximate ranges 1−20 and 90−129 are present on the capsid surface (shaded regions in Figure 2), while residues 20−90 are located in the interior of the capsid. Note that the points of contact between the capsid protein and RNA (filled diamonds in Figure 2) roughly correspond to amino acid residues that we classified as being located on the interior of the capsid (unshaded region in the figure).

Using the high-resolution structural information described above for MS2, it is possible to estimate the average surface charge density present on the viral surface under various assumptions. These estimates for the surface charge may then be compared to electrophoretic mobilities that we experimentally measured for MS2 in a previous study[1] and which are reproduced in Figure 3A. Comparisons of MS2 and λ pI values with other reported values for the whole-virus or outer surface proteins were also made in this earlier paper. Surface charge densities calculated from eq 5 are displayed in Figure 3B using the ionization constants either for isolated amino acids (open symbols) or for protein-embedded amino acids (solid symbols, see Experimental Section). The square symbols in Figure 3B represent the surface charge obtained when all of the charged residues in the polypeptide are considered. In this case, eq 5 predicts a net positive surface charge for MS2 over the pH range 3−9 and an extremely basic isoelectric point (pI > 9) that is inconsistent with the measured value (ca. 3.5). However, if this calculation is repeated using only those amino acid residues that are located on the capsid exterior (see shaded region in Figure 2 and discussion above), the resulting theoretical data (circles in Figure 3B) predict an isoelectric point that is in near perfect agreement with the measured value. This last calculation is strong evidence that the surface charge

(41) Cantor, C. R.; Schimmel, P. R. *Biophysical Chemistry, Part I: The Conformation of Biological Macromolecules*; W. H. Freeman and Co.: New York, 1980.
(42) Jou, M. W.; Haegeman, G.; Ysebaert, M.; Fiers, W. *Nature* **1972**, *237*, 92.
(43) Golmohammadi, R.; Vaelgard, K.; Gridborg, K.; Liljas, F. *J. Mol. Biol.* **1993**, *234*, 620.
(44) Valegard, K.; Liljas, L.; Fridborg, K.; Unge, R. *Nature* **1990**, *345*, 36.
(45) Kyte, J.; Doolittle, R. F. *J. Mol. Biol.* **1982**, *157*, 105.
(46) Valegard, K.; Murray, J. B.; Stockley, P. G.; Stonehouse, N. J.; Liljas, L. *Nature* **1994**, *371*, 623.

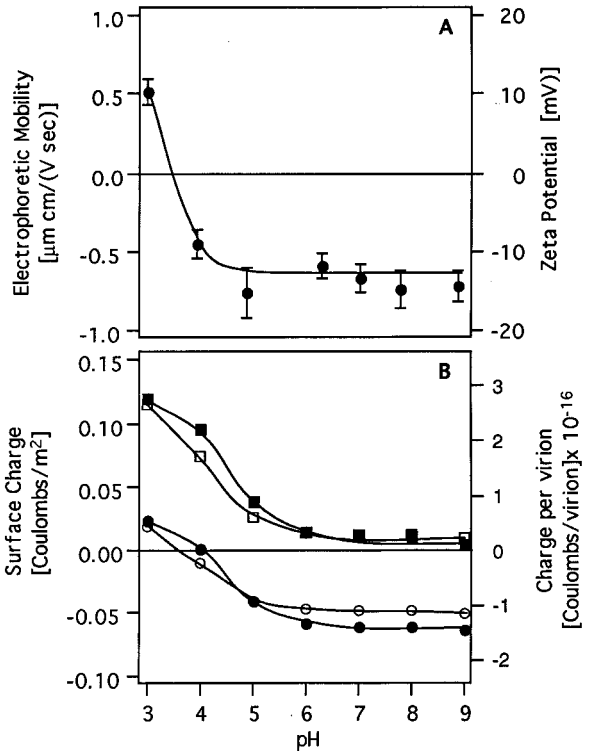

Figure 3. (A) Electrophoretic mobility and ζ potentials of MS2 in the presence of 0.01 M NaCl. (B) MS2 surface charge calculated from eq 5 using ionization constants either for single amino acids (open symbols) or for protein-embedded amino acids (filled symbols). Calculations were done taking into account all of the ionizable residues in the capsid protein (squares) or only those ionizable residues present on the capsid surface (circles).

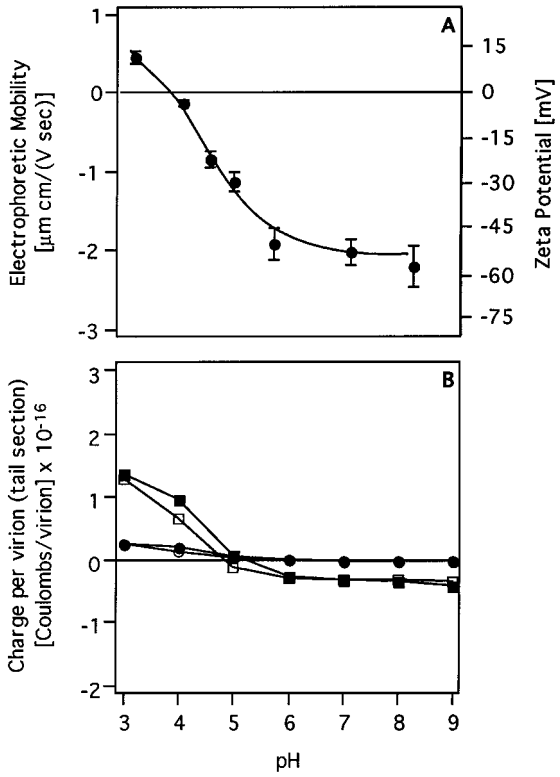

Figure 4. (A) Electrophoretic mobility and ζ potentials of λ in the presence of 0.01 M NaCl. (B) Charge per virion contributed by the tail tube (squares) and tail fiber (circles) calculated from eq 5, using ionization constants either for single amino acids (open symbols) or for protein-embedded amino acids (filled symbols). Calculations were done assuming only ionizable groups present on the exterior portions of the tail structure contribute surface charge (see Table 2).

on MS2 originates primarily from charged amino acid residues present on the exterior of the capsid surface. To our knowledge, this calculation represents the first attempt to directly relate the surface charge of a virus to its atomic-level three-dimensional structure.

We also carried out surface charge calculations (data not shown) in which the negative charge from the backbone of the viral RNA was included. The RNA molecule encapsulated inside MS2 consists of a linear single-stranded molecule approximately 4000 nucleotides in length. Even in the extremely unlikely event that 10% of the RNA was present on the viral surface, our calculations indicate that the p*I* of MS2 would be reduced by not more than 1 pH unit, relative to the case where only charged amino acid residues present on the surface of the virus are considered. This relative insensitivity of the calculated isoelectric point to the inclusion of negative charges from the RNA suggests that this molecule has little, if any, effect on the surface electrical properties of MS2.

Surface Properties of λ. Bacteriophage lambda (λ) is a structurally complex virus with an isometric head approximately 54 nm in diameter and a flexible tail tube 150 nm in length that terminates in a tail fiber approximately 25 nm long (see Figure 1). The head of λ is constructed from 405 copies of a single polypeptide referred to as gene product E, or "gpE", arranged on the capsid surface in icosahedral symmetry.[47] In addition to gpE, the capsid is also covered by 405 copies of a "decorating protein", gpD, that forms prominent protrusions on the capsid surface.[48] The atomic-scale three-dimensional structures of gpD and gpE have not yet been determined, so it is not currently possible to locate specific amino acid residues in these two polypeptides with respect to the exterior of the capsid, as was done for MS2 above. The tail tube of λ consists of 32 disks, each of which is composed of six copies of the polypeptide gpV. Genetic studies by Katsura and co-workers[49–51] suggest that gpV consists of an N-terminal domain which forms the interior core of the tail tube and a smaller C-terminal domain which loops off the surface. The tail fiber at the end of the tail tube is constructed from two to four copies of polypeptide gpJ, which, like gpV, appears to have two folding domains: an N-terminal doamin which anchors the fiber in the tail tube and a C-terminal domain which constitutes the portion of the tail fiber visible by electron microscopy.[52]

Figure 4A reproduces electrophoretic mobility data for λ from our earlier study[1] over the pH range from 3 to 9. The isoelectric point of λ is approximately 3.9, which is close to the value of 3.5 estimated for MS2 from Figure 3. By comparing the mobility data in Figures 3A and 4A, it is clear that λ is much more electronegative than MS2 for pH ≥ 5. At pH 5, for example, the calculated ζ potential for λ (−30 mV) is approximately 2 times larger in absolute magnitude than the ζ potential for MS2 (−15 mV).

Because detailed three-dimensional information is not available for the capsid proteins of λ, it is not currently possible to estimate the surface charge on the capsid

(47) Casjens, S.; Hendrix, R. *The Bacteriophages*; Calendar, R., Ed.; Plenum Press: New York, 1988; Vol. 2, pp 15–91.
(48) Dokland, T.; Murialdo, H. *J. Mol. Biol.* **1993**, *233*, 682.
(49) Katsura, I. *J. Mol. Biol.* **1981**, *146*, 493.
(50) Katsura, I.; Kobayashi, J. *J. Mol. Biol.* **1990**, *213*, 503.
(51) Katsura, I. In *Bacteriophage Assembly*; DuBow, M. S., Ed.; Alan R. Liss, Inc.: New York, 1981; pp 79–93.
(52) Haggard-Ljungquist, E.; Halling, C.; Calendar, R. *J. Bacteriol.* **1992**, *174*, 1462.

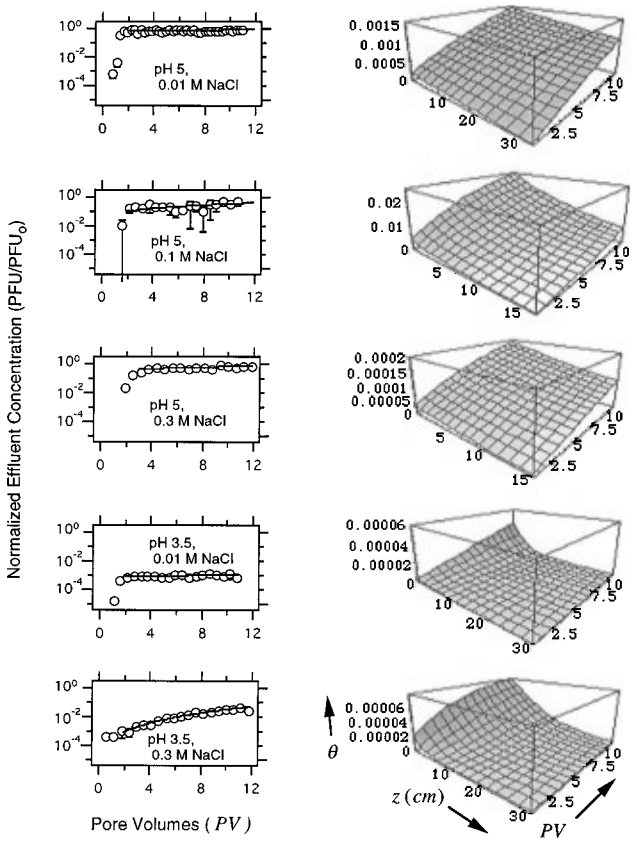

Figure 5. Panels on the left show MS2 breakthrough data (circles) and model predictions (lines) for filtration experiments conducted at the solution pH and NaCl concentrations noted. Error bars represent +/− one standard error. The panels on the right show model predictions for the fraction of the quartz surface occupied by deposited virus particles (θ) as a function of distance from the column influent (z) and pore volumes passed through the column (PV).

surface directly from amino acid sequence data. However, we were able to calculate the surface charge per virion contributed by the proteins which make up the tail structure of λ, namely, gpV and gp**J**. The results of these calculations are shown in Figure 4B for the tail tube (squares) and tail fiber (circles). As before, the open and solid symbols in this figure represent calculations based on ionization constants for, respectively, isolated and protein-embedded amino acids. The charge per virion contributed by these two polypeptides was calculated by using a modified form of eq 5 in which the parameter A was set equal to unity and by assuming only the charged residues present on the C-terminal domains, or "exterior" portions, of gpV and gp**J** contribute surface charge.

There are several important conclusions that can be derived from the calculations displayed in Figure 4B. First, the apparent isoelectric points for the tail tube and tail fiber (ca. 5) are more basic than the measured isoelectric point for the virus as a whole (ca. 3.9). This implies that at pH values between 3.9 and 5 the tail structure possesses a net positive charge, while the virus as a whole is negatively charged. Second, even at pH values above and below 5, the tail structure contributes relatively little charge to the overall virus ($<1.5 \times 10^{-16}$ C/virion). This is particularly evident for pH $\geq$ 5, where the charge per virion contributed by the tail is calculated to be less than 0.5×10^{-16} C in absolute magnitude. By contrast, the charge per virion contributed by the surface residues of the MS2 capsid protein is calculated to be in the range $(1-2) \times 10^{-16}$ C in absolute magnitude (see right hand axis of Figure 3B), even though the measured electrophoretic mobility of MS2 is less than the mobility of λ in this pH range. This suggests that most of the bulk surface electrical properties of λ are controlled by the surface of the capsid proteins rather than by the charge present on the tail. Taken together, these results also suggest that the surface of the λ head must (i) be highly negatively charged at pH $\geq$ 5 to account for the highly negative mobility observed for this virus in that pH range and (ii) have a relatively acidic isoelectric point (perhaps <3.9) to compensate for the relatively basic isoelectric point of the tail structure (ca. 5) and the measured isoelectric point for the virus as a whole (ca. 3.9).

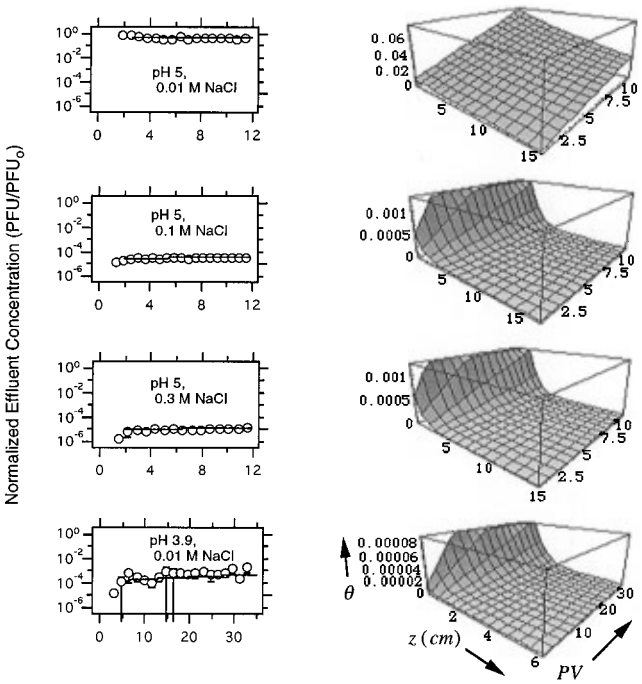

Figure 6. Breakthrough curves and predicted surface coverage for bacteriophage λ (see legend for Figure 5).

Filtration Experiments. In this section we present results for the interstitial transport of MS2 and λ through saturated packed beds of ultrapure quartz sand. These filtration data are interpreted in terms of the electrostatic and structural properties of the two viruses described in the previous section. Microelectrophoresis measurements on powdered samples of the quartz sand used in these experiments indicate that it has an isoelectric point between pH 2 and 3, which agrees well with previous streaming potential measurements involving similar packing material.[53] Most of the filtration experiments were conducted at pH 5 where MS2, λ, and the quartz sand all possess a net negative charge. An additional set of experiments were carried out at the isoelectric points of MS2 and λ—pH 3.5 and 3.9, respectively—to investigate their filtration under electrostatically favorable conditions. The ζ potentials of the quartz sand at pH 3.5, 3.9, and 5 in 0.01 M NaCl are approximately −6, −9, and −25 mV, respectively.[53] All experiments were conducted at 4 °C to minimize virus inactivation. In a set of initial experiments we determined that inactivation of MS2 and λ was not significant over the course of the filtration experiments at this temperature.[28]

The breakthrough curves (BTCs) for MS2 and λ are plotted against the cumulative pore volumes passed through the columns in Figures 5 and 6, respectively. Because of the remarkable sensitivity of the plaque-forming unit assay used to detect viruses in these experiments (lower limit of detection is approximately 10

(53) Litton, G. M.; Olson, T. M. *Environ. Sci. Technol.* **1993**, *27*, 185.

Table 2. Experimental Conditions and Fitting Parameters for Filtration Experiments Involving the Virus MS2[a]

experimental conditions						model fitting parameters				
pH	electrolyte	influent conc (PFU/mL)	ϵ	L (cm)	U_i (cm/s)	k_f (cm/s)	k_r (1/s)	χ^2	Q	α
5.0	0.010 M NaCl	1.7×10^7	0.47	34.3	0.053	2.5×10^{-6}	9.0×10^{-5}	60.1	0.003	0.009
5.0	0.10 M NaCl	3.3×10^8	0.45	17	0.055	2.4×10^{-5}	4.6×10^{-4}	17	0.3	0.09
5.0	0.30 M NaCl	3.3×10^6	0.43	16.5	0.057	1.0×10^{-5}	3.4×10^{-4}	31.5	0.003	0.04
3.5	0.010 M NaCl	4.4×10^6	0.48	34.9	0.052	3.3×10^{-5}	6.4×10^{-6}	22.3	0.1	0.12
3.5	0.30 M NaCl	4.6×10^5	0.47	32.4	0.053	4.2×10^{-5}	3.8×10^{-4}	38.4	0.001	0.16
5	0.30 M CsCl	6.2×10^5	0.45	16.5	0.058	N.D.	N.D.	N.D.	N.D.	N.D.

[a] N.D., not determined because the breakthrough was complete; i.e., PFU/PFU$_0 \approx 1$. χ^2 represents the minimum χ^2 value achieved during the nonlinear fitting routine, and Q represents the goodness of fit of the model. Values of $Q \geq 10^{-3}$ are generally considered to represent an acceptable fit.[30] The attachment efficiency, α, calculated from eq 2 is also shown for each experiment.

Table 3. Experimental Conditions and Fitting Parameters for the Filtration Experiments Involving the Virus λ[a]

experimental conditions						model fitting parameters				
pH	electrolyte	influent conc (PFU/mL)	ϵ	L (cm)	U_i (cm/s)	k_f (cm/s)	k_r (1/s)	χ^2	Q	α
5.0	0.010 M NaCl	4.7×10^8	0.44	16	0.057	7.9×10^{-6}	N.S.	27.3	0.02	0.045
5.0	0.10 M NaCl	1.5×10^8	0.46	17.5	0.055	9.4×10^{-5}	7.1×10^{-6}	2.5	1.0	0.53
5.0	0.30 M NaCl	1.2×10^8	0.43	15	0.061	1.2×10^{-4}	1.5×10^{-5}	13.5	0.6	0.65
3.9	0.010 M NaCl	3.0×10^6	0.44	6.2	0.057	2.2×10^{-4}	6.1×10^{-5}	21.5	0.16	1.25

[a] N.S., rejected as not statistically significant on the basis of the F-test (see text).

PFU/mL), normalized effluent concentrations as low as 10^{-6} can be easily measured with our experimental setup. In the following discussion we will focus on the nondispersive portion of the BTCs, which corresponds roughly to pore volumes greater than 2. The shape and magnitude of the virus BTCs shown in Figures 5 and 6 are sensitive to the pH and ionic composition of the pore fluid. For the set of experiments conducted with MS2 at pH 5 (top three panels in Figure 5), the nondispersive portion of the BTCs achieves a normalized breakthrough concentration in the range 0.1 < PFU/PFU$_0$ < 0.9, implying that fewer than 90% of the viruses in the column influent are retained on the quartz sand under these conditions. At this solution pH, the normalized PFU concentration at 10 mM NaCl is slightly higher than that at either 100 or 300 mM NaCl, although the influence of the salt concentration on the BTCs is not dramatic in this case. When the solution pH is lowered to coincide with the isoelectric point of MS2 (pH 3.5, bottom two panels in Figure 5), the normalized effluent concentration drops by several orders of magnitude and the shape of the BTCs becomes very sensitive to the concentration of NaCl. At 10 mM NaCl the normalized PFU concentration quickly attains a steady-state value of approximately 10^{-3}, implying that 99.9% of the viruses entering the column are retained in the column under these conditions. Raising the salt concentration to 300 mM leads to a continuous decrease in filter performance over time, presumably due to the desorption of viruses from the quartz media and/or blocking by previously deposited particles.[29]

In contrast to that of MS2, the normalized PFU concentration of bacteriophage λ at pH 5 is much more sensitive to the concentration of salt, decreasing from approximately 0.8 at 10 mM NaCl to 10^{-5} at 300 mM NaCl (top three panels in Figure 6). In this case, the normalized breakthrough concentration at the isoelectric point of λ (pH 3.9, bottom panel in Figure 6) is somewhat higher than the breakthrough concentrations observed at pH 5 and an NaCl concentration of either 100 or 300 mM.

To investigate the mechanisms responsible for virus filtration in our system, the nondispersive portions of the BTCs discussed above were fit to a mathematical model of virus transport through porous media which accounts for virus advection through the interstitial pores of the packed beds, first-order attachment of the viruses to the quartz grains at a rate k_f, and first-order detachment of the viruses from the quartz grains at a rate k_r (eq 1, see Experimental Section). The model does not account for virus inactivation, hydrodynamic dispersion, or the influence of previously deposited particles on the deposition rate, or "blocking". As discussed earlier, the first two processes are not important in our system because inactivation rates were negligible over the time scale of the filtration experiments and the transport of viruses in our system is advection dominated. To assess whether or not blocking plays an important role in our system, we carried out the following "modeling experiments". Values for the rate constants k_f and k_r were obtained by fitting the nondispersive portion of each BTC to an integrated form of eq 1, and these rate constants were then used in the model to predict the fraction of the quartz surface occupied by deposited viruses (θ). These model predictions for θ were compared with the observed BTCs to assess if the decrease in filter performance noted in some of our experiments correlated with high fractional surface coverage and hence was likely to be caused by blocking.

Tables 2 and 3 summarize the experimental conditions used for each column run and the corresponding rate constants k_f and k_r obtained by fitting the BTCs with eq 1. For one of the data sets (bacteriophage λ, pH 5, 10 mM NaCl) inclusion of the rate constant k_r in the fitting routine did not result in a statistically significant improvement in the χ^2 value (see Experimental Section), and therefore no value was reported for k_r in this particular case. The rate constants obtained from the nonlinear least-squares fitting routine were used to predict theoretical BTCs (shown as lines through the data points in Figures 5 and 6), and these predicted curves agree reasonably well with the observed data.

Three-dimensional plots of the predicted fractional surface coverage θ as a function of distance from the influent (z) and pore volumes passed through the column (PV) are shown adjacent to each of the BTCs in Figures 5 and 6. The spatial and temporal distribution of fractional surface coverage varied from experiment to experiment, depending primarily on the degree to which viruses were filtered and their influent concentration. Importantly, the experiment that exhibited the greatest loss in filter performance over time (bacteriophage MS2, pH 3.5, 300 mM NaCl) also has one of the lowest predicted surface coverages ($\theta \leq 10^{-5}$). Thus, virus desorption, and not blocking, appears to be responsible for the non-steady-state behavior of the BTC observed in this case. This

Table 4. Dimensionless Deposition Rates Estimated for λ and MS2

virus	η_0	η_0^{pI}
λ	2.81×10^{-2}	3.5×10^{-2}
MS2	4.29×10^{-2}	5.3×10^{-3}

conclusion also applies to the set of filtration experiments conducted with bacteriophage λ at pH 5. The predicted surface coverages for several of these experiments are relatively high, particularly near the column influent, yet none of the corresponding BTCs exhibit significant loss in filter performance over time. These results strongly suggest that if blocking occurs in our system, it is limited to a small region of the column near the influent and its impact on the BTCs is negligible.

The magnitude of the nondispersive portion of particle BTCs depends on the details of the experimental apparatus (e.g., packed bed length, interstitial fluid velocity, collector size, etc.) as well as the nature of attractive and/or repulsive forces occurring between the particles and the collector surface. Significant insight into the latter phenomenon can be obtained by recasting the filtration experiments in terms of a quantitative measure of virus−collector attachment rates referred to as the "attachment efficiency", or α. Physically, the attachment efficiency represents the fraction of colloid−collector collisions resulting in a sticking event, where in our case the "collector" represents the quartz packing material. Qualitatively, if particle−collector interactions are favorable, then the particles are rapidly filtered and $\alpha \rightarrow 1$; if particle−collector interactions are unfavorable, then the colloids remain largely in the pore fluid and $\alpha \ll 1$. Attachment efficiencies do not necessarily reflect virus mobility in porous media, however, because virus attachment may be reversible.

In order to calculate attachment efficiencies from each BTC, it was necessary to estimate the dimensionless deposition rate, η_0, for the two viruses. Physically, η_0 represents the fraction of viruses approaching the collector that collide with the surface. Theoretical values for η_0 calculated using the Smoluchowski−Levich ("S−L") approximation (eq 3, see Experimental Section) are displayed in Table 4. Also shown in this table are experimental estimates of the dimensionless deposition rate (η_0^{pI}) based on filtration experiments conducted at the isoelectric point of each virus (see eq 4). Reasonably close agreement between η_0 and η_0^{pI} was obtained for λ ($\eta_0^{pI}/\eta_0 = 1.25$). For comparison, differences of 100% between theoretical and experimental estimates of the deposition rate are not unusual, even when the colloids in question are well-characterized polystyrene microspheres.[54] The S−L approximation assumes that the colloids in question are spherical, and therefore the agreement between η_0 and η_0^{pI} in the case of λ may indicate that the deposition rate is not influenced by the nonspherical geometry of this particular virus. In contrast to that for phage λ, the experimental deposition rate estimated for MS2 is more than 800% less than theoretical estimates of η_0 ($\eta_0^{pI}/\eta_0 = 0.12$, see Table 4). This difference between experimentally and theoretically derived values of η_0 is outside of the range typical for packed column experiments and suggests that one or more nonelectrostatic repulsive forces enhance the transport of MS2 at the p*I* of the virus.

Attachment Efficiencies for MS2 and λ. The magnitude of the attachment efficiency α was calculated from eq 2 using the forward rate constants k_f listed in Tables 2 and 3 and the theoretical estimates of η_0 listed in Table 4. We focused on the set of MS2 and λ experiments conducted at pH 5. At this solution pH, MS2, λ, and the quartz surface are negatively charged, and therefore these experiments were conducted under conditions where repulsive electrostatic double layer (EDL) forces may affect deposition rates.

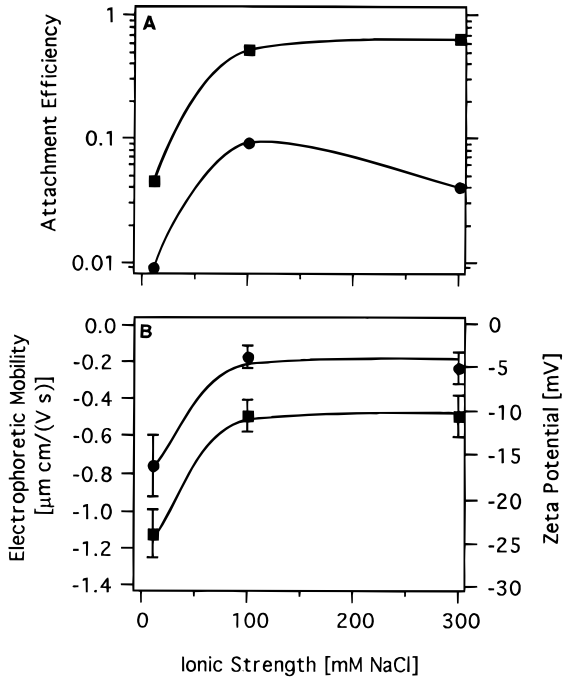

Figure 7. (A) Attachment efficiencies measured for λ (squares) and MS2 (circles) at pH 5 as a function of ionic strength. (B) Electrophoretic mobilities measured for λ (squares) and MS2 (circles) at pH 5 and a range of salt concentrations. The mobility values for MS2 are reproduced from Penrod et al.;[1] the mobility values for λ were measured in this study. The lines in this figure are drawn to emphasize data trends and do not represent model predictions.

Figure 7A displays the influence of salt concentration on virus attachment efficiency for bacteriophage λ (squares) and MS2 (circles). For comparison, the electrophoretic mobility of these two viruses is shown in Figure 7B over the same range of salt concentrations. At pH 5, the salt concentration strongly influences both the surface electrical potential of the viruses and their attachment efficiencies. At 10 mM NaCl, both MS2 and λ possess large negative surface potentials (ζ potentials of −17 and −22 mV, respectively) and are poorly filtered by the packed beds of granular quartz (attachment efficiencies of 0.0094 and 0.045, respectively). As the salt concentration is increased from 10 to 100 mM NaCl, there is a decrease in the magnitude of the surface potential of the viruses and a parallel increase in their attachment efficiency. Presumably, the surface potential of the viruses decreases with increasing salt concentration due to compression of the electrostatic double layer surrounding the virus particles. This reduction in the surface potential leads to a decrease in the repulsive EDL force acting between the virus and the quartz surface and to an overall increase in the virus attachment efficiency, consistent with DLVO theory as applied to the filtration of lyophobic colloids.[55] Increasing the salt concentration further from 100 to 300 mM NaCl has little impact on λ's attachment efficiency but does appear to cause a decrease in the value of α measured for MS2 (see Figure 7A). A similar reduction

(54) Elimelech, M.; O'Melia, C. R. *Environ. Sci. Technol.* **1990**, *24*, 1528.

(55) Lyklema, J. In *The Scientific Basis of Flocculation*; Ives, K. J., Ed.; Sitjhoff and Noordhoff: The Netherlands, 1978; pp 3−36.

in the attachment efficiency at high salt concentrations was noted by Elimelech[54,56] for the filtration of small (46 nm diameter) latex spheres through packed columns of glass beads. This researcher attributed the anomalous decrease in α at high ionic strength (either 300 mM KCl or >10 mM $CaCl_2$) to repulsive hydration forces. The possibility that hydration forces also inhibit MS2 deposition onto the quartz sand is investigated later in this work.

Another interesting feature of these filtration data is the significant difference in the attachment efficiencies observed for λ and MS2 at high salt. Repulsive EDL forces should become negligible when salt concentrations exceed 200 mM, and therefore α should approach unity as the salt concentration approaches and/or exceeds this value. This prediction is consistent with the data for phage λ in Figure 7A, suggesting that repulsive EDL forces effectively dominate the deposition kinetics of this particular virus under the solution conditions examined here. The α value measured for MS2, on the other hand, is significantly less than unity at 300 mM NaCl (see Figure 7A) or at the isoelectric point of the virus (see previous section). Thus, in the case of MS2, the deposition kinetics appear to be influenced by repulsive EDL forces at low salt concentration and by another (nonelectrostatic) repulsive force at high ionic strength. The possibility that this nonelectrostatic force is "steric" in nature is examined in the following section.

Modeling Interaction Forces for MS2. On the basis of an examination of the three-dimensional structure of the coat protein (see Figure 4 in Valegard *et al.*[44]), there are two polypeptide structures on the MS2 surface which might give rise to steric repulsive forces, including a relatively long hairpin loop which connects the βA and βB sheets and a shorter loop connecting the αA and αB helices (residues 11−17 and 113−116 in Figure 2, respectively). Referring to Figure 2, both of these polypeptide structures are relatively hydrophilic (negative hydropathy values), suggesting that their interaction with a collector surface would involve primarily repulsive steric interactions.

To determine if the steric stabilization energies arising from the longer βA−βB loops are sufficient to account for the low deposition rates observed for MS2 at high salt concentrations (300 mM) or the reversible deposition of MS2 at its p*I*, we estimated the steric and London−van der Waals interaction energy profiles as a function of separation distance. Electrostatic repulsive interaction energies were assumed to be negligible at these solution conditions.

Theoretical estimates of the dimensionless van der Waals interaction energies, V_{vdW}, can be obtained from the approximate expression developed by Gregory[57] for sphere−plate interactions,

$$V_{vdW} = \frac{A_{132} a_p}{6h(1 + 14h/\omega)} \quad (6)$$

where a_p is the radius of the virus, h is the MS2−quartz grain separation distance, A_{132} is the effective Hamaker constant for the MS2−water−quartz system, and ω is the characteristic wavelength of interaction, which is usually taken as 100 nm. The Hamaker constant for the polio virus−water−quartz interaction has been estimated as $A_{132} = 4 \times 10^{-21}$ J by Murray and Parks[18] using Lifshitz theory[58] and with the assumption that polio virus and polystyrene have similar dielectric properties. Interaction energy calculations in this study were performed by assuming that the value of A_{132} obtained by Murray and Parks represents an upper-limit Hamaker constant for the MS2−water−quartz system. Keesom and Debye dipolar contributions to van der Waals interactions are screened in the presence of concentrated electrolyte solutions. Marra,[59] for example, has used direct force measurements to demonstrate that the nonretarded Hamaker constant for two interacting uncharged lipid bilayers decreases from approximately 7×10^{-21} J in pure water to 3×10^{-21} J in 0.1 M NaCl. A range of Hamaker constants from 1×10^{-21} to 4×10^{-21} J, therefore, was considered to determine whether such effects might explain the greater reversibility of attachment at the p*I* of MS2 in 0.3 M NaCl solutions.

The total steric interaction energy between a polymer-coated particle and an uncoated flat plate consists of two components: a repulsive osmotic energy term, V_{osm}, that is due to the exclusion of water molecules surrounding the polymers on the close particle−surface approach and an elastic repulsive energy, V_{elas}, that arises as polymer chains are compressed and their configurational entropy decreases. An expression for the dimensionless osmotic interaction energy was derived by Amirbahman,[60] on the basis of earlier work of Napper and co-workers:[61]

$$V_{osm} = \frac{(2 \times 10^{-14})\pi a_p \Phi_2^2 N_A}{\bar{V}_1}(1/2 - \chi_1)(\delta - h)^2 \quad (7)$$

where Φ_2 is the volume fraction of the polymer, N_A is Avogadro's number, $\bar{V}_1$ is the molar volume of the solvent, χ_1 is the Flory−Huggins solvency parameter, and δ is the thickness of the polymer coating. The volume fraction was estimated from the number of βA−βB loops present on the surface of each virion (180), the presumed length of the polypeptide loop (see below), and consensus values for the hydrated volume of each amino acid residue present in the loop structure.[62] On the basis of a polypeptide segment length of 0.34 nm per amino acid residue for the loop connecting the βA and βB sheets,[63] the maximum distance this loop could extend off of the capsid surface is approximately 1 nm, or $\delta = 1$ nm. Hydropathy values for this loop structure (residues 11−17 in Figure 2) indicate that the loop is relatively hydrophilic. Other relatively hydrophilic polymers, such as poly(ethylene oxide) and poly(vinyl alcohol), have χ_1 values in the range 0.46−0.47.[64,65] In estimating the V_{osm} contribution to the overall energy of interaction between MS2 and quartz, a slightly wider range of χ_1 values from 0.45 to 0.49 was considered.

Analytical expressions for the V_{elas} term were derived by Evans *et al.*[66] for several types of polymer segment density distributions. For a sphere−plate interaction in which polymer is present on only one of the surfaces the following expression for V_{elas} is obtained:

(56) Elimelech, M. *J. Chem. Soc., Faraday Trans.* **1990**, *86*, 1623.
(57) Gregory, J. *J. Colloid Interface Sci.* **1981**, *83*, 138.
(58) Nir, S. *Prog. Surf. Sci.* **1976**, *8*, 1.
(59) Marra, J. *J. Colloid Interface Sci.* **1986**, *109*, 11.
(60) Amirbahman, A. Unpublished Ph.D. Dissertation, University of California, Irvine, 1994.
(61) Napper, D. H. *J. Colloid Interface Sci.* **1977**, *58*, 390.
(62) Perkins, S. J. *Eur. J. Biochem.* **1986**, *157*, 169.
(63) Schultz, G. E.; Schirmer, R. H. *Principles of Protein Structure*; Springer-Verlag: New York, 1979; p 69.
(64) Einarson, M. B.; Berg, J. C. *J. Colloid Interface Sci.* **1993**, *155*, 165.
(65) Vincent, B.; Luckham, P. F.; Waite, F. A. *J. Colloid Interface Sci.* **1980**, *73*, 508.
(66) Evans, R.; Smitham, J. B.; Napper, D. H. *Colloid Polym. Sci.* **1977**, *255*, 161.

$$V_{elas} = \frac{2 \times 10^{-14} \pi a_p N_A \Phi_2 \delta^2 \rho_2}{M} \times \left\{\frac{2}{3} - \frac{1}{6}\left(\frac{h}{\delta}\right)^3 - \left(\frac{h}{2\delta}\right) + \frac{h}{\delta} \ln \frac{h}{\delta}\right\} \quad (8)$$

where ρ_2 and M are the density and molecular weight of the polymer, respectively. The values of these parameters were taken as $\rho_2 = 1.947$ g cm^{-3} and $M = 760.7$ g mol^{-1}.

Figure 8 represents the total interaction energy profiles ($V_{tot} = V_{vdW} + V_{osm} + V_{elas}$) calculated from eqs 6−8 for the parameter values noted in the figure legend and the ranges of χ_1 and A_{132} discussed above. The profiles obtained by assuming full extension of the loops, $\delta = 1$ nm (Figure 8a and c), are also compared with a case in which the loops extend only 0.75 nm from the capsid surface (Figure 8b and d). All of the interaction energy profiles exhibit a shallow secondary minimum ranging from $-0.5kT$ to $-3kT$ at $h \approx \delta$. The depth of the minimum increases as the value of A_{132} increases and as δ decreases; it was insensitive to the choice of the χ_1 used in the model. Importantly, none of these profiles exhibit an energy barrier to the deposition of MS2 in the secondary minimum, suggesting that the attachment rate of MS2 to the quartz sand should be transport-limited. This result is not consistent with our earlier observation that the experimentally determined k_f values at high salt or at the p*I* of the virus are significantly smaller (>800% less) than predictions based on the S−L approximation. An explanation for this discrepancy is not apparent, although it should be noted that the interaction energy expressions employed here probably oversimplify the nature of virus−quartz interactions over the very small separation distances examined in Figure 8. Therefore, it is conceivable that an energy barrier to deposition in the secondary minimum, if it exists, might not be captured by the current modeling effort. Also, it should be pointed out that the S−L approximation has not been tested, to our knowledge, with other particles as small as MS2. As Figure 8c and d demonstrates, the depth of the secondary minimum well decreases as the virus−water−quartz Hamaker constant decreases. Screening of the van der Waals force at high salt concentrations, therefore, could account for the greater reversibility of MS2 observed at the p*I* (see bottom two panels in Figure 5 and the corresponding reverse rate constants in Table 2).

As mentioned earlier, it is possible that hydration forces are responsible for the anamolously low deposition rates observed for MS2 at high salt concentrations or at the p*I* of the virus. In the presence of salt, hydrated cations may bind to the negatively charged surfaces of the quartz and the virus. At small particle−collector separations (<1 nm), the water molecules surrounding these cations must reorder themselves, and this entropically unfavorable process gives rise to a repulsive interaction force. It is possible to probe the significance of these forces by using salt cations with different hydration numbers or number of bound water molecules per cation. In particular, repulsive hydration forces should increase with the hydration number of the cation. In the set of filtration experiments reported in Figure 7A, for example, sodium was used as the cation. Sodium is relatively hydrated, with a hydration number of 4−5.[67] We repeated one of the filtration experiments (pH 5, 300 mM ionic strength) using the relatively less-hydrated cesium cation (hydration number 1−2). If hydration forces are important in this system, we expected that the filtration efficiency of MS2

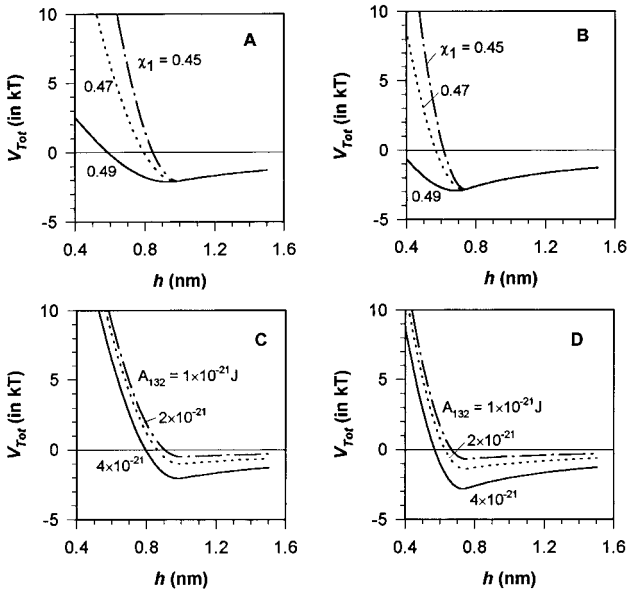

Figure 8. Total interaction energy profiles calculated for the MS2−water−quartz system. (A) $A_{132} = 4 \times 10^{-21}$, $\delta = 1$ nm, $\Phi_2 = 0.047$; (B) $A_{132} = 4 \times 10^{-21}$, $\delta = 0.75$ nm, $\Phi_2 = 0.064$; (C) $\chi_1 = 0.47$, $\delta = 1$ nm, $\Phi_2 = 0.047$; (D) $\chi_1 = 0.47$, $\delta = 0.75$ nm, $\Phi_2 = 0.064$.

in the presence of cesium would be greater than that in the presence of sodium, or $\alpha_{Cs} > \alpha_{Na}$. However, when sodium was replaced with cesium, we found that MS2 exhibited complete breakthrough (see Table 2), and hence the attachment efficiency was less in the presence of cesium than in the presence of sodium. Hydration forces, therefore, cannot account for the low deposition rate observed for MS2 at high salt concentration.

Deposition Mechanisms for *λ*. Some important mechanistic conclusions can also be drawn regarding the role that both tail and capsid must play in influencing the deposition kinetics of bacteriophage λ. On the basis of surface charge calculations and measured electrophoretic mobilities, we concluded earlier that the λ capsid and tail have, respectively, a net negative and zero surface charge at pH 5. The localization of negative charge on the λ capsid at pH 5 suggests that there exists a strong electrostatic barrier for capsid−quartz interactions at low ionic strength. Even under these electrostatically unfavorable conditions, however, it is conceivable that the uncharged and relatively flexible tail structure might "tether" λ particles to the quartz surface. Instead, we observed very low deposition rates of λ at pH 5 and low salt concentrations (see top panel in Figure 6 and Figure 7A), perhaps because the electrostatic repulsive force acting between the capsid and collector is too long range under these conditions to permit anchoring of the particle through tail−collector interactions alone.

At high ionic strength we found that the deposition kinetics of λ approached the S−L limit (i.e., $\alpha \approx 1$, see Figure 7A). It is interesting to speculate why steric repulsive forces do not appear to mobilize λ at high ionic strength, despite the fact that gpD and gpE form prominent protrusions on the λ capsid (see Figure 1). One possible explanation is that steric repulsive forces act over relatively short distances ($\leq$1−2 nm). In the absence of long-range electrostatic repulsive interactions between the capsid head and the quartz surface, perhaps the λ capsid can get close enough to the quartz surface for the tail to play a more important role in tethering the virus to the collector. Alternatively, it is possible that the attractive van der Waals forces exerted by λ are greater than those for MS2, especially since λ is a larger particle

(67) Israelachvili, J. *Intermolecular and Surface Forces*, 2nd ed.; Academic Press: New York, 1992; pp 55 and 56.

and the van der Waals interaction energy is proportional to the particle radius for sphere−plate interactions (see eq 6). In this case, repulsive steric interaction forces would also be less effective in mobilizing λ at high salt concentrations.

Conclusions

In this work, we investigated the surface electrical properties of the two bacteriophages MS2 and λ and their interstitial transport in a model porous medium consisting of ultrapure quartz sand. The electrokinetic behavior of MS2 could be readily interpreted in terms of its three-dimensional surface molecular structure. Our observation that only the exterior charge groups present on the MS2 capsid influence its electrophoretic mobility suggests that, in general, both the acidity *and position* of these groups influence the surface electrical properties of viruses, and ultimately, their filtration rates.

Different repulsive interaction forces for MS2 and λ were invoked to explain the solution chemistry dependence of their deposition kinetics. Electrostatic forces appear to dominate the deposition rate of λ, whereas both electrostatic and nonelectrostatic interaction forces appear to regulate the deposition kinetics of MS2. Hydration forces were ruled out as the possible "nonelectrostatic force", at least for pH 5 and 300 mM ionic strength, because less filtration was observed when Na^+ was replaced with the relatively less hydrated Cs^+ cation. The possibility that polypeptide loops on the particle surface give rise to steric repulsive forces was evaluated by calculating interaction energy profiles based on a balance of attractive van der Waals and repulsive steric interactions. These profiles predict that virus deposition occurs in a secondary minimum the depth of which is relatively sensitive to the value of the presumed Hamaker constant. Hence, it is possible that the greater reversibility observed for MS2 at its isoelectric point and high ionic strength may be due to screening of the Keesom and Debye dipolar contributions to the van der Waals interactions. However, the profiles fail to predict the anamolously low deposition rates observed at high salt or the p*I* of MS2, and it is not clear whether this failure is due to limitations in the interaction energy expressions or the involvment of some other (i.e., nonsteric) nonelectrostatic force. If steric interactions are responsible for the mobility of MS2 when electrostatic interactions are suppressed, it is striking that steric forces do not also play a role in mobilizing λ. The fact that different repulsive forces appear to be operative for the two viruses examined here can be attributed to a number of factors, including (i) a smaller surface charge on MS2 relative to the λ capsid, (ii) favorable interactions of the λ tail with the bed media, or (iii) differences in the effective Hamaker constant for MS2− and λ−water−quartz systems.

One practical impact of this work concerns the proposal that bacteriophages be used as "surrogates" for viruses of genuine human health concern in ground water transport studies.[68−70] The basic idea is that male-specific coliphages, such as MS2, are often naturally present in sources of human waste like septic tank effluents, and thus their presence or absence in ground water may be an indicator of water purity. Currently, the suitability of a particular virus as a surrogate is judged on the basis of its relative insensitivity to inactivation,[71,72] its ecological similarity to human pathogens,[73] and its gross morphological resemblance to human enteric viruses known to cause waterborne disease like Norwalk virus and rotavirus. The present study suggests that relatively subtle aspects of viral surface structure—such as the presence of polypeptide loops and the distribution of ionizable amino acid residues—can significantly influence the rate at which viruses are removed from the water phase by filtration. Thus, it is unlikely that any single bacteriophage will adequately mimic the transport behavior of viral pathogens in ground water, particularly given that the surface structures of different waterborne human viruses are quite dissimilar.[74]

Acknowledgment. The authors would like to thank H. W. Walker for reviewing the manuscript and Prof. M. Elimelich at UCLA for performing numerical simulations of dimensionless deposition rates. This material is based upon work supported by the National Water Research Institute and the U.S. Environmental Protection Agency under Award NWRI/EPA 92-04.

Glossary

A	surface area of the virus (cm^2)
A_s	Happel's dimensionless packing parameter (−)
A_{132}	Hamaker constant for the interaction of material 1 with material 2 through medium 3
a_g	radius of the collector grains (cm)
a_p	radius of the virus particle (cm)
D_∞	diffusion coefficient of colloid in bulk solution (cm^2/s)
F	Faraday's constant, 1.6×10^{-15} C/charge
h	sphere−plate separation distance (nm)
kT	thermal energy (J)
k_f	forward rate constant for virus attachment (cm/s)
k_f^{pI}	forward rate constant for virus attachment determined at the isoelectric point for the virus (cm/s)
k_r	reverse rate constant for virus detachment (1/s)
L	length of the packed bed (cm)
M	molecular weight of the polymer (g/mol)
N	number of polypeptides per viral particle (−)
N_A	Avogadro's number, 6.023×10^{23}
n	fluid concentration of infective virus particles (PFU/mL)
n_s	surface concentration of infective virus particles (PFU/cm^2)
PFU	number of infective virus particles expressed in terms of plaque-forming units (−)
PFU_0	number of PFUs present in a sample taken from the column influent (−)
$pK_a^{a.a}$	acidity constant for an isolated amino acid (−)
pK_a^{prot}	acidity constant for an amino acid embedded in a protein (−)
Q	goodness-of-fit corresponding to the minimum χ^2

(68) Snowdon, J. A.; Cliver, D. O. *Crit. Rev. Environ. Control* **1989**, *19*, 231.
(69) IAWPRC Study Group on Health Related Water Microbiology. *Water Resour. Res.* **1991**, *25*, 529.
(70) Reddy, K. R.; Khaleel, R.; Overcash, M. R. *J. Environ. Qual.* **1981**, *10*, 255.
(71) Yates, M. V.; Gerba, C. P.; Kelley, L. M. *Appl. Environ. Microbiol.* **1985**, *49*, 778.
(72) Yates, M. V.; Yates, S. R.; Warrick, A. W.; Gerba, C. P. *Appl. Environ. Microbiol.* **1986**, *52*, 479.
(73) Havelaar, A. H.; Olphen, M. V.; Drost, Y. C. *Appl. Environ. Microbiol.* **1993**, *59*, 2956.
(74) Blacklow, N. R.; Greenberg, H. B. *N. Engl. J. Med.* **1991**, *325*, 252.

value obtained by nonlinear least-squares fitting (−)

R_iH^+ number of positively charged residues associated with the "*i*th" type of amino acid (−)

R_iO^- number of negatively charged residues associated with the "*i*th" type of amino acid (−)

s_v projected area of a virus particle (cm^2)

t time (s)

U superficial velocity (cm/s)

U_i interstitial particle velocity (cm/s)

V_{elas} dimensionless elastic interaction energy (−)

V_{osm} dimensionless osmotic interaction energy (−)

V_{tot} dimensionless total interaction energy (−)

V_{vdW} dimensionless van der Waals interaction energy (−)

$\bar{V}_l$ molar volume of solvent (cm^3)

z distance from column influent (cm)

α fraction of colloid−collector collisions which result in sticking, or "attachment efficiency" (−)

χ^2 weighted sum-of-square difference between model predictions and observed data, or "chi-square", used in the nonlinear fitting routine (−)

χ_1 Flory−Huggins solvency parameter (−)

δ polymer coating thickness (nm)

ϵ packed bed porosity (−)

η_0 fraction of colloids approaching a collector that collide with the collector, or "dimensionless deposition rate" (−)

η_0^{pI} experimental estimate for η_0 determined at the isoelectric point of the virus (−)

θ fraction of collector surface area occupied by deposited virus particles (−)

ρ_2 density of the polymer (g/cm^3)

σ specific surface charge on the virus (C/m^2)

ω characteristic wavelength of the van der Waals interaction (nm)

Φ_2 volume fraction of the polymer (−)

LA950884D